Stability via symmetry breaking in interacting driven systems

Andrew Pocklington [1,2,*] and Aashish A. Clerk [2]

[1]*Department of Physics, University of Chicago, 5640 South Ellis Avenue, Chicago, Illinois 60637, USA*
[2]*Pritzker School of Molecular Engineering, University of Chicago, Chicago, Illinois 60637, USA*

Photonic and bosonic systems subject to incoherent, wide-bandwidth driving cannot typically reach stable finite-density phases using only nondissipative Hamiltonian nonlinearities; one instead needs nonlinear losses, or a finite pump bandwidth. We describe here a very general mechanism for circumventing this common limit, whereby Hamiltonian interactions can cut-off heating from a Markovian pump, by effectively breaking a symmetry of the unstable, linearized dynamics. We analyze two concrete examples of this mechanism. The first is a new kind of $\mathcal{PT}$ laser, where Hermitian Hamiltonian interactions can move the dynamics between the $\mathcal{PT}$ broken and unbroken phases and thus induce stability. The second uses on-site Kerr or Hubbard type interactions to break the chiral symmetry in a topological photonic lattice, inducing exotic phenomena from topological lasing to the stabilization of Fock states in a topologically protected edge mode.

I. INTRODUCTION

The competition between pumping, loss, and interactions are a ubiquitous feature of both classical and quantum nonlinear dynamics. The often complex interplay between incoherent pumping (which tends to drive a system towards an infinite temperature state) and a nonlinearity that can cut off heating instabilities leads to a rich variety of physics. Examples include classical limit cycles and lasers in the few body regime [1,2], classical synchronization [3,4], and driven-dissipative phase transitions in many body systems [5–8] (e.g., effective Mott insulator to superfluid transitions in driven bosonic lattice systems [9–12]).

The simplest form of the above interplay arises when the incoherent pumping has a finite bandwidth. In this case, instability can be prevented with Hamiltonian interactions or nonlinearities that shift system excitation energies with increasing density. This naturally cuts off heating and stabilizes a finite density state, as higher excited states will become non-resonant with the pump, see Fig. 1(a). Such bandwidth-limited pumping has been exploited to realize an effective chemical potential for light, and requires coupling to a non-Markovian (or finite bandwidth) dissipative reservoir [10,13,14]. Realizing such setups in many-body settings is generally challenging (though see Ref. [12] for a recent experiment). If one instead is restricted to completely broadband (Markovian) pumping, then conventional wisdom dictates that Hamiltonian interactions are irrelevant, as pumping is insensitive to system energies [c.f., Fig. 1(b)]. In this case, one expects that a heating instability can only be prevented by nonlinear loss. Paradigmatic examples here are the van der Pol oscillator [15], as well standard oscillator/laser gain-saturation mechanisms [1,2].

The two above routes would seem to exhaust the set of generic mechanisms for having nonlinearities (either Hamiltonian or dissipative) cut off pumping-induced instabilities. Here, we show that this is surprisingly not the case: there is a third extremely generic mechanism that allows Hamiltonian interactions to stabilize systems driven by a broadband (Markovian) pump. The trick here is not to make use of energy shifts (as the pump is insensitive to energies in this limit), but instead exploit symmetry, see Fig. 1. As we demonstrate in detail, by making use of symmetries that can be effectively broken as a function of excitation density, Hamiltonian interactions combined with incoherent broadband pumping can stabilize finite-density states. More concretely, we show that certain systems are sensitive to incoherent pumping only because of symmetries of the effective low-density dynamics. By adding a nonlinearity that breaks these symmetries as particle density increases, we obtain a highly effective mechanism for stabilizing finite density states, one that is distinct from more standard approaches.

To illustrate our ideas, we first analyze a quantum version of the well-studied parity-time ($\mathcal{PT}$) symmetric gain-loss dimer [16,17]. While stabilization here is usually achieved via nonlinear dissipation, we show that a purely Hamiltonian approach is also possible: a finite density phase can be stabilized by introducing non-dissipative quartic nonlinearities. The result is a new kind of $\mathcal{PT}$ laser, e.g., [18–22]. We then turn to more complex many-body bosonic lattice systems subject to Markovian pumping, showing that the combination of a chiral sublattice symmetry and standard on-site Kerr (or Hubbard) interactions allows one to stabilize finite-density states. This mechanism is especially interesting for systems supporting topological edge modes [23], as it enables a new kind of topological lasing [24–28] and the stabilization of nonclassical, topological light [29,30], e.g., single-photon Fock states in a topological edge mode [31]. Surprisingly, this can occur even in the limit of very weak interactions.
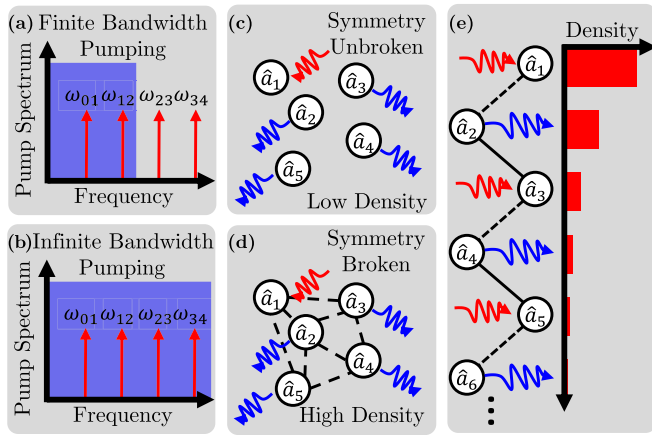
*abpocklington@uchicago.edu

FIG. 1. (a) Standard mechanism for obtaining stable states in interacting bosonic systems subject to a finite-bandwidth, incoherent pump: transition frequencies increase with increasing excitation number, eventually having no overlap with the pump spectrum (blue). (b) This mechanism fails for a Markovian, infinite-bandwidth pump. (c) A set of orbitals/normal modes, where one mode is guaranteed by some symmetry to experience only pumping (red arrow, $\hat{a}_1$), while the remaining modes are lossy (blue arrows). The low-density phase is thus unstable. (d) A symmetry-breaking interaction forces the modes to hybridize at high photon density, leading to a stable finite-density state. (e) By subjecting a topological SSH chain to staggered pumping and loss, symmetry breaking interactions can induce topological lasing, with an exponentially localized steady state photon density.

II. $\mathcal{PT}$ SYMMETRY

We first consider a parity-time ($\mathcal{PT}$) symmetric dimer: two bosonic modes $\hat{a}$, $\hat{b}$ with a tunnel Hamiltonian $\hat{\mathcal{H}}_0 = J(\hat{a}^\dagger \hat{b} + \hat{b}^\dagger \hat{a})$, with $\hat{a}$ ($\hat{b}$) experiencing Markovian loss (gain) at a rate κ_a (κ_b). The quantum dynamics of the system's density matrix $\hat{\rho}$ is described by a Lindblad master equation [32,33]:

$$\dot{\hat{\rho}} = -i[\hat{\mathcal{H}}_0, \hat{\rho}] + \kappa_a \mathcal{D}[\hat{a}]\hat{\rho} + \kappa_b \mathcal{D}[\hat{b}^\dagger]\hat{\rho}, \qquad (1)$$

where $\mathcal{D}[\hat{L}]\hat{\rho} \equiv \hat{L}\hat{\rho}\hat{L}^\dagger - \frac{1}{2}\{\hat{L}^\dagger\hat{L}, \hat{\rho}\}$. This system has been studied extensively in both classical [16,22] and quantum [34,35] settings, and undergoes a $\mathcal{PT}$ breaking transition when J drops below $J_c = \frac{1}{4}(\kappa_a + \kappa_b)$, becoming dynamically unstable when $J \leqslant \frac{1}{2}\sqrt{\kappa_a\kappa_b}$. This has a simple intuitive explanation: for small J, $\mathcal{PT}$ is broken and eigenmodes localize, hence the eigenmode localized on b can become unstable as it primarily experiences gain. When instead $J \gg \kappa_a, \kappa_b$, $\mathcal{PT}$ is unbroken and eigenmodes delocalize. Assuming that $\kappa_a > \kappa_b$, this means both eigenmodes experience net loss, making them dynamically stable.

In the regime $2J < \sqrt{\kappa_a\kappa_b}$, the system is dynamically unstable, and a nonlinearity is needed to restore stability. In a standard $\mathcal{PT}$ laser, this would be done by adding nonlinear dissipation which causes the gain to saturate at a large photon number (see, e.g., Refs. [18,34]). Here, we propose an alternative stabilization mechanism that only uses a *Hamiltonian* interaction which restores $\mathcal{PT}$ as the number of excitations increases. This requires a nonlinear hopping $J \to \tilde{J}(n)$ where the hopping strength grows monotonically with the total photon number n. We consider $\hat{\mathcal{H}}_{\text{int}} = \frac{J}{2}\frac{\hat{n}}{n^*}(\hat{a}^\dagger\hat{b} + \hat{b}^\dagger\hat{a})$ where $\hat{n} \equiv$

$\hat{a}^\dagger\hat{a} + \hat{b}^\dagger\hat{b}$, and n^* a dimensionless constant setting the scale of the nonlinearity. The total Hamiltonian is thus

$$\hat{\mathcal{H}} \equiv \hat{\mathcal{H}}_0 + \hat{\mathcal{H}}_{\text{int}} = J\left(1 + \frac{1}{2}\frac{\hat{n}}{n^*}\right)(\hat{a}^\dagger\hat{b} + \hat{b}^\dagger\hat{a}). \qquad (2)$$

Note that similar density-dependent tunneling interactions have been studied in a variety of different contexts (e.g., Refs. [36–38]).

We study the resulting master equation dynamics using a standard mean-field decomposition, see Appendix A 1. This yields the equations of motion:

$$\dot{n}_a = \tilde{J}c - \kappa_a n_a, \quad \dot{n}_b = -\tilde{J}c + \kappa_b n_b + \kappa_b, \qquad (3)$$

$$\dot{c} = 2\tilde{J}(n_b - n_a) - \frac{\kappa_a - \kappa_b}{2}c, \qquad (4)$$

where we have defined the density dependent hopping $\tilde{J}(n_a, n_b) = J[1 + 1/(2n^*)] + J(n_a + n_b)/n^*$, the local densities $n_a \equiv \langle \hat{a}^\dagger\hat{a} \rangle$, $n_b \equiv \langle \hat{b}^\dagger\hat{b} \rangle$, and the current $c \equiv i\langle a^\dagger b - b^\dagger a \rangle$. Note that in this mean-field approximation, the interaction acts exactly as expected, where the coupling strength increases linearly with the total number of photons in the cavity. The bare coupling strength is increased by a factor of $\frac{1}{2n^*}$ which are related to the zero point fluctuations coming from the canonical commutation relations. The equations can be solved self-consistently, and show that as expected, our Hamiltonian nonlinearity always stabilizes the system in regimes where the linear dynamics is unstable. Making a Gross-Pitaevskii approximation, one can solve for the expected coherent state amplitudes $a, b = |\langle \hat{a} \rangle|^2, |\langle \hat{b} \rangle|^2$ in the steady state as (see Appendix A 2)

$$\frac{|a|^2 + |b|^2}{2n^*} = 0 \quad J \geqslant \frac{1}{2}\sqrt{\kappa_a\kappa_b},$$

$$\frac{|a|^2 + |b|^2}{2n^*} = \frac{\sqrt{\kappa_a\kappa_b}}{2J} - 1 \quad J \leqslant \frac{1}{2}\sqrt{\kappa_a\kappa_b}, \qquad (5)$$

indicating a lasing transition when $2J = \sqrt{\kappa_a\kappa_b}$. We give an analytic expression for the stability conditions, as well as phase diffusion in the finite density regime in Appendix A 2. We also find that the mean-field description gives a good approximation to exact master equation numerics in the regime of large density, see Appendix A 4.

We stress that there are significant qualitative and quantitative differences between our Hamiltonian stabilization route to $\mathcal{PT}$ lasing versus approaches based on standard gain saturation [1,34]. In a conventional $\mathcal{PT}$ laser [18,21], the gain is naturally cutoff at large photon values, i.e. the gain rate depends on the number of photons in the gain mode, $\kappa_b \equiv \kappa(1 + \langle \hat{n}_b \rangle/n_{crit})^{-\nu}$ for some $\nu > 0$ [34]. Such a *dissipative* nonlinearity can of course stabilize almost *any* kind of pumping-induced instability (i.e., one is effectively just turning down the pumping strength with increasing density). As such, for this conventional route to stability, the presence or absence of $\mathcal{PT}$ is largely irrelevant.

In marked contrast to this, the $\mathcal{PT}$ symmetry of the linearized dynamics is critical to stabilization in our nonlinear hopping model. When $\kappa_a = \kappa_b \equiv \kappa$, if one breaks the $\mathcal{PT}$ symmetry by adding a relative detuning δ, $\hat{\mathcal{H}} \to \hat{\mathcal{H}} + \delta(\hat{a}^\dagger\hat{a} - \hat{b}^\dagger\hat{b})$, a standard $\mathcal{PT}$ laser with gain saturation experiences almost no qualitative changes, see Appendix A 3. Alternatively,

the nonlinear hopping model introduced here immediately becomes unstable when there is a nonzero detuning. This behavior is independent of the nonlinearity strength, and reflects the fact that with a nonzero δ, it is no longer possible to dynamically tune the system between the $\mathcal{PT}$ broken and unbroken phases by varying density. This stark difference is shown in Fig. 5. The strong sensitivity to δ in our setup could potentially be harnessed for a new kind of non-Hermitian sensing modality [39–45].

III. CHIRAL SYMMETRY

We now consider a more general version of our stabilization mechanism, where the relevant interactions break a purely Hamiltonian symmetry at nonzero densities. We will consider the example of photons hopping on a lattice with a chiral symmetry, and use on-site Kerr nonlinearities (i.e., Hubbard interactions U) to provide the requisite symmetry breaking. Note that this is distinct from previous studies exploring the consequences of squeezed dissipation in chiral bosonic lattices having linear dynamics [46–50]. Our work involves no squeezing, and is focused on *nonlinear* dynamics (something not treated in these previous works).

Let $\hat{\mathcal{H}}_0$ be a quadratic Hamiltonian that has a chiral sublattice symmetry $\hat{\mathcal{U}} : \hat{\mathcal{U}}\hat{\mathcal{H}}_0\hat{\mathcal{U}}^\dagger \mapsto -\hat{\mathcal{H}}_0$. Examples include nearest-neighbor tight-binding models on any bipartite lattice. A particularly simple example is a 1D lattice $\hat{\mathcal{H}}_0 = \sum_i J_i\hat{a}_i^\dagger\hat{a}_{i+1} + \text{H.c.}$ The chiral symmetry here is $\hat{\mathcal{U}} : \hat{\mathcal{U}}\hat{a}_i\hat{\mathcal{U}}^\dagger \mapsto (-1)^i\hat{a}_i$. More generically, such a chiral symmetry defines two sublattices A, B. If we have local annihilation operators $\hat{a}_i \in A$ and $\hat{b}_i \in B$, then

$$\hat{\mathcal{U}}\hat{a}_i\hat{\mathcal{U}}^\dagger = \hat{a}_i, \quad \hat{\mathcal{U}}\hat{b}_i\hat{\mathcal{U}}^\dagger = -\hat{b}_i. \tag{6}$$

We consider a setup where we apply very weak incoherent pumping (gain) with a rate $\eta^2\kappa$ ($\eta \ll 1$) on the A sublattice, and loss with a rate κ on the B sublattice. This is described by the Lindblad master equation:

$$\dot{\rho} = -i[\hat{\mathcal{H}}, \hat{\rho}] + \kappa\left(\sum_i \eta^2\mathcal{D}[\hat{a}_i^\dagger] + \mathcal{D}[\hat{b}_i]\right)\hat{\rho} \tag{7}$$

with $\hat{\mathcal{H}} = \hat{\mathcal{H}}_0 + \hat{\mathcal{H}}_{\text{int}}$. The hopping Hamiltonian $\hat{\mathcal{H}}_0$ can be diagonalized as $\hat{\mathcal{H}}_0 = \sum_\alpha \epsilon_\alpha \hat{d}_\alpha^\dagger \hat{d}_\alpha$. By making suitable unitary rotations of the jump operators, we can rewrite the dissipative part of the master equation as

$$\sum_i \mathcal{D}[\hat{a}_i^\dagger] = \frac{1}{4}\sum_\alpha \mathcal{D}[\hat{d}_\alpha^\dagger + \hat{\mathcal{U}}\hat{d}_\alpha^\dagger\hat{\mathcal{U}}^\dagger], \tag{8}$$

$$\sum_i \mathcal{D}[\hat{b}_i] = \frac{1}{4}\sum_\alpha \mathcal{D}[\hat{d}_\alpha - \hat{\mathcal{U}}\hat{d}_\alpha\hat{\mathcal{U}}^\dagger], \tag{9}$$

using nothing more than the chiral symmetry Appendix B 2. Note that $\hat{\mathcal{U}}\hat{d}_\alpha\hat{\mathcal{U}}^\dagger$ is necessarily also an eigenmode annihilation operator with energy $-\epsilon_\alpha$.

Consider first the case where there are no interactions, and $\hat{\mathcal{H}}_0$ has a nonzero spectral gap Δ ($|\epsilon_\alpha| > \Delta > 0$) such that $\kappa \ll \Delta$. We can then approximate $\mathcal{D}[\hat{d}_\alpha^{(\dagger)} \pm \hat{\mathcal{U}}\hat{d}_\alpha^{(\dagger)}\hat{\mathcal{U}}^\dagger] \sim \mathcal{D}[\hat{d}_\alpha^{(\dagger)}] + \mathcal{D}[\hat{\mathcal{U}}\hat{d}_\alpha^{(\dagger)}\hat{\mathcal{U}}^\dagger]$. Each mode thus experiences a net decay rate $\kappa(1 - \eta^2)/2 \sim \kappa/2$, and the dissipative steady state is simple: each mode will be in a thermal state with average

photon number

$$n_{th} = \frac{\eta^2}{1 - \eta^2} \ll 1. \tag{10}$$

The physics is more interesting in the case where $\hat{\mathcal{H}}_0$ has $n > 0$ zero energy eigenmodes $\hat{d}_{0,i}$, $i = 1, \ldots, n$, that are mapped to themselves by the chiral symmetry, $\hat{\mathcal{U}}\hat{d}_{0,i}\hat{\mathcal{U}}^\dagger = \hat{d}_{0,i}$. Eqs. (8) and (9) imply that these modes will *only* experience incoherent pumping and not any loss. These modes are thus unstable regardless of how small η is, with a gain rate of $\eta^2\kappa$. Intuitively, this is a consequence of the zero modes' wave functions only having support on the A sublattice.

We now introduce on-site Kerr (Hubbard) interactions:

$$\hat{\mathcal{H}}_{\text{int}} = \frac{U}{2}\sum_i (\hat{a}_i^\dagger\hat{a}_i^\dagger\hat{a}_i\hat{a}_i + \hat{b}_i^\dagger\hat{b}_i^\dagger\hat{b}_i\hat{b}_i). \tag{11}$$

This interaction explicitly breaks the chiral sublattice symmetry. Hence, at a mean-field level (where we describe the system with a self-consistent quadratic Hamiltonian), the interaction will cause the unstable, symmetry protected zero modes to hybridize with the stable lossy modes as the dynamics drives the system from low to high density. This hybridization will induce loss into the original unstable modes, leading ultimately to a stable, finite-density state. In what follows, we give a specific example of this mechanism in a lattice with a protected topological edge mode, showing that the mean-field picture sketched here is accurate at large photon density and predicts topological lasing. We further show that the mechanism also works in non-mean-field low density regimes, leading to edge states stabilized in non-classical states.

IV. TOPOLOGICAL LASING

Generating a lasing transition in a photonic lattice where only a topological edge lases is a difficult engineering challenge. Many solutions often require injecting extremely narrowband pumping at the edge-mode frequency [25,51]. Our symmetry-breaking stabilization mechanism opens a new pathway for realizing this goal using completely broadband, Markovian pumping. We will consider a concrete example of a 1D bosonic Su-Schrieffer-Heeger (SSH) chain [52,53], something that has been realized in a variety of experimental platforms, including superconducting circuits [54], micropillar polariton cavities [26], photonic cavities [55], ring resonators [27,28,56], and optomechanics [57]. With an odd number of sites, this lattice has a single, topologically protected, zero energy edge mode, where the topology is protected by the chiral sublattice symmetry. The noninteracting Hamiltonian is

$$\hat{\mathcal{H}}_{\text{SSH}} = -J\sum_{i=1}^{N-1}(1 - \delta)\hat{a}_i^\dagger\hat{b}_i + (1 + \delta)\hat{b}_i^\dagger\hat{a}_{i+1}+, \tag{12}$$

where $-1 < \delta < 1$. This system is in a topological regime when $\delta > 0$, and there exists a single zero energy edge mode that lives on only the A sublattice (i.e., $n = 1$).

Following our general recipe, we apply incoherent pumping to the A sublattice and loss to the B sublattice. Such
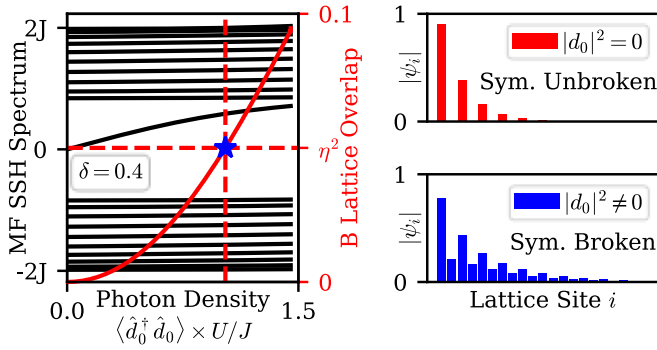
FIG. 2. Left. Spectrum (solid black lines) and edge-mode overlap with the B sublattice (solid red) for a mean-field description of our driven-dissipative SSH model, where the effective Hamiltonian is density dependent. Interactions and pumping generate self-consistent on-site energies Δ_i, modifying the spectrum and wave functions. When the B-lattice overlap matches the gain to loss ratio η^2, the dynamics achieves stability. This then determines the steady state photon density (dashed red lines). Right: Wave-function profile of the edge mode in mean-field theory when $U|d_0|^2 = 0$ (upper) and $U|d_0|^2 = 1.4$ (lower). When the steady state density is 0 chiral symmetry is unbroken, and the edge-mode wave function vanishes on the B sublattice. As the density increases, the chiral symmetry is broken, causing the edge mode to have overlap with both sublattices. In all plots we have taken $N = 21$ sites, and $\delta = 0.4$.

FIG. 3. (a) Exact steady-state photon density for a five- site driven-dissipative interacting SSH chain [c.f., Eqs. (7) and (12)] with $U = \kappa = J$, $\xi = 10^{-2}$, and $\eta = \xi^2$. Despite the global, Markovian pumping in the system, the photonic density is strongly localized at the left edge. The inset depicts the first five sites of an SSH chain where solid (dashed) lines represent strong (weak) bonds. Even (odd) numbered sites experience loss shown with blue arrows (gain, red arrows), and each site has a local Kerr nonlinearity. (b) Steady state total photon number versus the pump to loss ratio η obtained from mean-field theory (red) and from exact numerics (blue). Exact numerics asymtote to 1 photon in the weak pump limit as it approaches a Fock state in the edge mode for $\eta \lesssim \xi^2$ (dashed vertical line). Here, $U = 0.1$, $\xi = 10^{-3}$, $\kappa = J = 1$. (c) (In)fidelity to a single photon Fock state in the topological edge mode for $\xi = 10^{-1}$ (black), 10^{-2} (blue), and 10^{-3} (red) versus the nonlinearity U. Here, $\kappa = J = 1$, $\eta = \xi^2$.

localized, incoherent pumping can be achieved experimentally by, e.g., coupling a site $\hat{a}_i$ to a lossy auxilliary reservoir $\hat{c}$ via a coherent squeezing interaction ($\hat{\mathcal{H}} = g\hat{a}_i\hat{c} +$ H.c.). If the auxilliary cavity has a loss rate $\Gamma \gg g$, tracing out the auxilliary cavity gives the effective dynamics $\frac{4g^2}{\Gamma}\mathcal{D}[\hat{a}_i^\dagger]$, as desired.

We will again consider an interaction $\hat{\mathcal{H}}_{\text{int}} = \frac{U}{2}\sum_i \hat{a}_i^\dagger\hat{a}_i^\dagger\hat{a}_i\hat{a}_i + \hat{b}_i^\dagger\hat{b}_i^\dagger\hat{b}_i\hat{b}_i$. The full master equation is then given by Eq. (7) with $\hat{\mathcal{H}} = \hat{\mathcal{H}}_{\text{SSH}} + \hat{\mathcal{H}}_{\text{int}}$. This corresponds to a specific example of a driven-dissipative SSH Bose-Hubbard chain, with alternating gain and loss.

The semiclassical (Gross-Pitaevskii) equations for the dynamics of $a_i \equiv \langle\hat{a}_i\rangle$, $b_i \equiv \langle\hat{b}_i\rangle$ are given by

$$\dot{a}_i = -iJ(1+\delta)b_i - i(1-\delta)b_{i-1} - iU|a_i|^2 a_i + \frac{\kappa\eta^2}{2}a_i,$$

$$\dot{b}_i = -iJ(1+\delta)a_i - i(1-\delta)a_{i+1} - iU|b_i|^2 b_i - \frac{\kappa}{2}b_i. \quad (13)$$

We can then define a set of self-consistent on-site potentials Δ_i and a real space wave-function ψ_i (see Appendix B 1 for more details):

$$\Delta_i = U|\psi_i|^2|d_0|^2, \quad (14)$$

$$\sum_j [(H_{\text{SSH}})_{ij} + \Delta_i\delta_{ij}]\psi_j = \lambda\psi_i. \quad (15)$$

d_0 is the self-consistent edge mode amplitude (which depends on the local on-site energy Δ_i), and $(H_{\text{SSH}})_{ij}$ the single-particle SSH Hamiltonian matrix. As can be seen in Fig. 2, as the self-consistent on-site energy $U|d_0|^2 \equiv \sum_i \Delta_i$ is increased from zero (i.e., the photon density increases), the overlap of the self-consistent edge mode on the lossy B sublattice
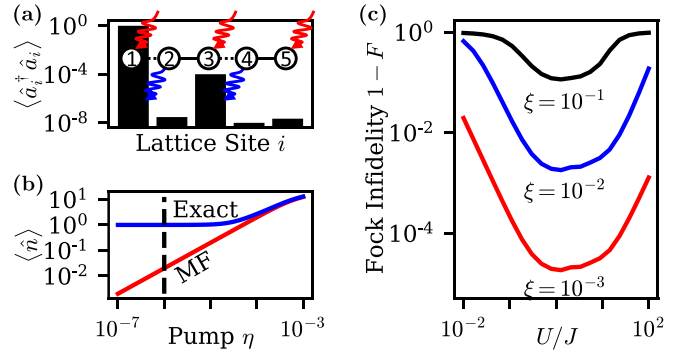
also increases, reflecting the breaking of chiral symmetry and inducing stability in this mode. This delocalization leads to a finite-density steady state. For weak κ, the corresponding density is found by the value of $U|d_0|^2$ that makes the spatial overlap of the edge mode on the B-lattice exactly η^2 (the pumping to loss ratio). The breaking of chiral symmetry also causes the edge mode to acquire a nonzero energy [c.f. Fig. 2]. As a result, we obtain a stable limit cycle where the zero mode oscillates at the self-consistent frequency generated by the Kerr nonlinearity, see Appendix B 1.

V. TOPOLOGICAL FOCK STATES

In parameter regimes we are able to test numerically, the semiclassical analysis of Eq. (7) is accurate if the stabilized photon number is large. However, the stabilization mechanism is not limited to these parameter regimes. Consider our driven SSH chain in the regime where $U \sim J \sim \kappa$, and the dimensionless pumping parameter η is chosen so that semiclassics would predict a steady state with $\mathcal{O}(1)$ photons in the edge mode. In this regime, we show that it is possible to instead stabilize a single photon Fock state in the edge, where the steady state density matrix can be approximated as $\hat{\rho}_{ss} \sim \hat{d}_0^\dagger|0\rangle\langle 0|\hat{d}_0 \equiv \hat{\rho}_1$, with $|0\rangle$ the vacuum and $\hat{d}_0$ the annihilation operator of the symmetry-protected edge mode, see Fig. 3(a). It has been a long-standing challenge to engineer nonclassical light in a topological edge mode [31], and the proposed stabilization mechanism provides an alternative method.

To understand the origin of this effect, we first define the ratio between weak and strong bonds $\xi \equiv (1-\delta)/(1+$

δ), which is related to the localization length ξ_L by $\xi_L = -[\log \xi]^{-1}$. We write the pumping rate parameter η in Eq. (7) as $\eta \equiv \eta' \xi^2$. Consider the physics in the strong localization case where $\xi \to 0$ while $\eta' = \mathcal{O}(1)$ stays fixed. To leading order in ξ^2, we find that the steady state is exactly a Fock state, that is

$$\hat{\rho}_{ss} = \hat{d}_0^\dagger |0\rangle\langle 0| \hat{d}_0 + \mathcal{O}(\xi^2), \tag{16}$$

see Appendix B 4 for a derivation. This is shown in Fig. 3(c). This is intimately related to the stabilization mechanism: because the linear dynamics are unstable, and the discreteness of the nonlinearity means that it only acts nontrivially when there are at least two photons in the lattice, the quantum dynamics can *never* stabilize fewer than a single photon in the steady state Appendix B 4, see Fig. 3(b). The upshot is that one can stabilize a Fock state to arbitrary accuracy in this regime by choosing ξ appropriately.

Despite the fact that the steady state in this case only has density in a single mode, we stress the fact that the physics here cannot be captured by any simple effective single-mode theory, e.g., single photon pumping and two-photon loss (see Appendix B 4). The stabilization mechanism is completely reliant on the fact that the edge mode is able to weakly hybridize with the stable bulk modes as the photon density increases. Furthermore, our numerically exact master equation simulations show that our Fock state stabilization mechanism is extremely robust against variations. The nonlinearity can be an order of magnitude weaker than the loss rate and the quadratic Hamiltonian ($U \ll \kappa, J$) with little impact on the final fidelity, see Fig. 3(c). This is a further potential advantage of our method: it can generate Fock states with extremely weak nonlinearities.

VI. CONCLUSION

In this paper, we have both introduced and analyzed a new generic method that allows nondissipative Hamiltonian interactions and nonlinearities to stabilize finite density phases in bosonic systems subject to broadband, incoherent pumping. The mechanism does not rely on energetics, but instead uses the ability of interactions to effectively break symmetries at finite density. Our method is highly adaptable, and represents a generic mechanism for using incoherent, Markovian pumping and Hamiltonian nonlinearities to stabilize finite density phases of matter in bosonic lattices (including nonclassical states such as Fock states). This would not be possible using previously known mechanisms, which require nonlinear loss to stabilize infinite bandwidth pumping. While we focused here on chiral symmetry, we expect that our mechanism can also be used to stabilize topological lasing in lattice models protected by different kinds of symmetry.

Note added: During the final preparation of this work, we became aware of Ref [58], which identified a related mechanism for selectively populating edge modes in a noninteracting fermionic model. Note that the physics in the fermionic case is very different, as unlike bosons, there is no possibility of dynamical instabilities, hence finite density states of driven setups emerge generically even without interactions or nonlinearity.

APPENDIX A: $\mathcal{PT}$ SYMMETRY

1. Mean field solution

Consider the model proposed in the main text, given by

$$\hat{\mathcal{H}} = J\left(1 + \frac{\hat{n}}{2n^*}\right)(\hat{a}^\dagger \hat{b} + \hat{b}^\dagger \hat{a}), \tag{A1}$$

$$\hat{L}_1 = \sqrt{\kappa_a}\hat{a}, \qquad \hat{L}_2 = \sqrt{\kappa_b}\hat{b}^\dagger. \tag{A2}$$

We can calculate the time evolution of operator averages using the adjoint Liouvillian $\partial_t\langle\hat{O}\rangle = \langle i[\hat{\mathcal{H}}, \hat{O}] + \frac{1}{2}\sum_i[\hat{L}_i^\dagger, \hat{O}]\hat{L}_i + \hat{L}_i^\dagger[\hat{O}, \hat{L}_i]\rangle$. We define photon number operators $\hat{n}_a = \hat{a}^\dagger\hat{a}$, $\hat{n}_b = \hat{b}^\dagger\hat{b}$, and the current operator $\hat{c} \equiv i(\hat{a}^\dagger\hat{b} - \hat{b}^\dagger\hat{a})$. Note that the operator $\hat{a}^\dagger\hat{b} +$ h.c. is conserved by the Hamiltonian dynamics, and so it decays to zero in the steady state. We can calculate that

$$\partial_t\langle\hat{n}_a\rangle = -J\left\langle\left(1 + \frac{\hat{n}}{2n^*}\right)\hat{c}\right\rangle - \kappa_a\langle\hat{n}_a\rangle, \tag{A3}$$

$$\partial_t\langle\hat{n}_b\rangle = J\left\langle\left(1 + \frac{\hat{n}}{2n^*}\right)\hat{c}\right\rangle + \kappa_b\langle\hat{n}_b\rangle + \kappa_b, \tag{A4}$$

$$\partial_t\langle\hat{c}\rangle = -2J\left\langle\left(1 + \frac{\hat{n}}{2n^*}\right)(\hat{n}_a - \hat{n}_b)\right\rangle - \frac{\kappa_a - \kappa_b}{2}\langle\hat{c}\rangle. \tag{A5}$$

At this point, what we have is exact, but the equations do not close on themselves (i.e., the RHS involves three- and four-point averages). To make progress, we make a Gaussian approximation, and evaluate correlators on the RHS by ignoring higher cumulants (i.e., we assume that Wick's theorem holds). This yields

$$\langle\hat{n}\hat{c}\rangle = i\langle\hat{a}^\dagger\hat{a}\hat{a}^\dagger\hat{b}\rangle + i\langle\hat{b}^\dagger\hat{b}\hat{a}^\dagger\hat{b}\rangle - i\langle\hat{a}^\dagger\hat{a}\hat{b}^\dagger\hat{a}\rangle - i\langle\hat{b}^\dagger\hat{b}\hat{b}^\dagger\hat{a}\rangle$$
$$= (2\langle\hat{n}\rangle + 1)\langle\hat{c}\rangle, \tag{A6}$$

and

$$\langle\hat{n}(\hat{n}_a - \hat{n}_b)\rangle = \langle\hat{n}_a^2\rangle - \langle\hat{n}_b^2\rangle = (2\langle\hat{n}\rangle + 1)\langle\hat{n}_a - \hat{n}_b\rangle. \tag{A7}$$

Putting everything together, this gives us the result quoted in the main text:

$$\partial_t\langle\hat{n}_a\rangle = -J\left\langle 1 + \frac{\hat{n} + 1/2}{n^*}\right\rangle\langle\hat{c}\rangle - \kappa_a\langle\hat{n}_a\rangle, \tag{A8}$$

$$\partial_t\langle\hat{n}_b\rangle = J\left\langle 1 + \frac{\hat{n} + 1/2}{n^*}\right\rangle\langle\hat{c}\rangle + \kappa_b\langle\hat{n}_b\rangle + \kappa_b, \tag{A9}$$

$$\partial_t\langle\hat{c}\rangle = -2J\left\langle 1 + \frac{\hat{n} + 1/2}{n^*}\right\rangle\langle\hat{n}_a - \hat{n}_b\rangle - \frac{\kappa_a - \kappa_b}{2}\langle\hat{c}\rangle. \tag{A10}$$

2. Semiclassical stability analysis and phase noise

The mean-field analysis above allowed us to derive an equation of motion that corresponded to a density dependent

hopping. We can similarly consider a semiclassical equation of motion for the field operators $a \equiv \langle \hat{a} \rangle$, $b \equiv \langle \hat{b} \rangle$ starting from Eqs. (A1) and (A2). This gives

$$\dot{a} = iJ\left(1 + \frac{|a|^2 + |b|^2}{2n^*}\right)b + \frac{iJa}{2n^*}(a^*b + b^*a) - \frac{\kappa_a}{2}a, \tag{A11}$$

$$\dot{b} = iJ\left(1 + \frac{|a|^2 + |b|^2}{2n^*}\right)a + \frac{iJb}{2n^*}(a^*b + b^*a) + \frac{\kappa_b}{2}b. \tag{A12}$$

We can simplify this significantly by recalling that in the full quantum system, we know that $\langle \hat{a}^\dagger \hat{b} + \hat{b}^\dagger \hat{a} \rangle$ is always zero in the steady state and conserved by the Hamiltonian. We therefore will neglect the term $(a^*b + b^*a)$ in the equations of motion (which does not affect the fixed point or stability), to get the much simpler dynamical system of equations

$$\partial_t a = -iJ\left(1 + \frac{|a|^2 + |b|^2}{2n^*}\right)b - \frac{\kappa_a}{2}a, \tag{A13}$$

$$\partial_t b = -iJ\left(1 + \frac{|a|^2 + |b|^2}{2n^*}\right)a + \frac{\kappa_b}{2}b. \tag{A14}$$

Note that in this form, the nonlinearity acts identically to the mean-field case, where the coupling J scales with density. We can calculate the steady state populations analytically, which gives two solutions, recovering the result from the main text:

$$\frac{n}{2n^*} = 0, \qquad \frac{n}{2n^*} = \frac{\sqrt{\kappa_a \kappa_b}}{2J} - 1. \tag{A15}$$

It is trivial to observe that below threshold, when $\sqrt{\kappa_a \kappa_b} < 2J$, the first solution is dynamically stable, as in this case the

nonlinearity does not affect the linear stability analysis. We will next show that in the lasing regime $\sqrt{\kappa_a \kappa_b} > 2J$, the other solution is dynamically stable.

It is worth noting that the absolute phase of the modes is unconstrained by the fixed point equations, reflecting the $U(1)$ symmetry inherent in the problem. In a real laser, noise would cause this free phase to diffuse, which we can model using the Langevin equations

$$\partial_t a = -iJ\left(1 + \frac{|a|^2 + |b|^2}{2n^*}\right)b - \frac{\kappa_a}{2}a + \sqrt{\kappa_a}\xi_a, \tag{A16}$$

$$\partial_t b = -iJ\left(1 + \frac{|a|^2 + |b|^2}{2n^*}\right)a + \frac{\kappa_b}{2}b + \sqrt{\kappa_b}\xi_b, \tag{A17}$$

where $\langle \xi_{a,b}(t)\xi_{a,b}^*(t') \rangle = \delta(t - t')$ are complex white noise operators. We will expand the equations of motion about the fixed point and define

$$a = (\rho_a + \delta\rho_a)e^{i\phi}, \quad \rho_a^2 = 2n^* \frac{\kappa_b}{\kappa_a + \kappa_b}\left(\frac{\sqrt{\kappa_a \kappa_b}}{2J} - 1\right), \tag{A18}$$

$$b = i(\rho_b + \delta\rho_b)e^{i(\phi + \delta\phi)}, \quad \rho_b^2 = 2n^* \frac{\kappa_a}{\kappa_a + \kappa_b}\left(\frac{\sqrt{\kappa_a \kappa_b}}{2J} - 1\right). \tag{A19}$$

Here, $\delta\rho_{a,b}$ are the fluctuating densities of the a, b modes, respectively, which we will show are constrained to be zero in the steady state without any noise. The relative phase $\delta\phi = 0$ as well in the steady state, with ϕ the free absolute phase. Making the approximation that $\delta\rho_{a,b}/\rho_{a,b}, \delta\phi \ll 1$, we can linearize the equations of motion about the stable fixed point to get:

$$e^{-i\phi}\dot{a} = \dot{\delta\rho_a} + i\dot{\phi}(\rho_a + \delta\rho_a)$$
$$= J\left(1 + \frac{(\rho_a + \delta\rho_a)^2 + (\rho_b + \delta\rho_b)^2}{2n^*}\right)(\rho_b + \delta\rho_b)e^{i\delta\phi} - \frac{\kappa_a}{2}(\rho_a + \delta\rho_a) + \sqrt{\kappa_a}e^{-i\phi}\xi_a, \tag{A20}$$

$$-ie^{-i(\phi + \delta\phi)}\dot{b} = \dot{\delta\rho_b} + i(\dot{\phi} + \dot{\delta\phi})(\rho_b + \delta\rho_a)$$
$$= -J\left(1 + \frac{(\rho_a + \delta\rho_b)^2 + (\rho_b + \delta\rho_b)^2}{2n^*}\right)(\rho_a + \delta\rho_a)e^{-i\delta\phi} + \frac{\kappa_b}{2}(\rho_b + \delta\rho_b) + \sqrt{\kappa_b}e^{-i(\phi + \delta\phi)}\xi_b. \tag{A21}$$

From here, it is simple to define the new (real valued) white noise variables $\xi_a' = \text{Im } e^{-i\phi}\xi_a$, $\xi_a'' = \text{Re } e^{-i\phi}\xi_a$ and $\xi_b' = \text{Im } e^{-i(\phi + \delta\phi)}\xi_b$, $\xi_b'' = \text{Re } e^{-i(\phi + \delta\phi)}\xi_b$. By taking the real part of Eqs. (A20) and (A21), we can show that, to linear order, the densities will be stable around the fixed point by looking at the linearized dynamics:

$$\dot{\delta\rho_a} = \left(\frac{\sqrt{\kappa_a \kappa_b}}{2} + \frac{\kappa_a}{\kappa_a + \kappa_b}(\sqrt{\kappa_a \kappa_b} - 2J)\right)\delta\rho_b + \left(\frac{\sqrt{\kappa_a \kappa_b}}{\kappa_a + \kappa_b}(\sqrt{\kappa_a \kappa_b} - 2J) - \frac{\kappa_a}{2}\right)\delta\rho_a + \sqrt{\kappa_a}\xi_a'', \tag{A22}$$

$$\dot{\delta\rho_b} = -\left(\frac{\sqrt{\kappa_a \kappa_b}}{2} + \frac{\kappa_b}{\kappa_a + \kappa_b}(\sqrt{\kappa_a \kappa_b} - 2J)\right)\delta\rho_a - \left(\frac{\sqrt{\kappa_a \kappa_b}}{\kappa_a + \kappa_b}(\sqrt{\kappa_a \kappa_b} - 2J) - \frac{\kappa_b}{2}\right)\delta\rho_b + \sqrt{\kappa_b}\xi_b''. \tag{A23}$$

This corresponds to a dynamical matrix whose eigenvalues are

$$-\frac{\kappa_a^2 - \kappa_b^2}{4\kappa_a \kappa_b}\left(1 \pm \sqrt{1 + \frac{16\sqrt{\kappa_a \kappa_b}}{(\kappa_a - \kappa_b)^2}(2J - \sqrt{\kappa_a \kappa_b})}\right), \tag{A24}$$

which are negative definite if and only if $2J - \sqrt{\kappa_a \kappa_b} < 0$ as desired. Similarly, we can take the imaginary part of Eqs. (A20) and (A21) to show that

$$\dot{\phi} = \frac{\kappa_a}{2}\delta\phi + \frac{\sqrt{\kappa_a}}{\rho_a}\xi_a', \tag{A25}$$

$$\dot{\delta\phi} = -\frac{\kappa_a - \kappa_b}{2}\delta\phi + \frac{\sqrt{\kappa_b}}{\rho_b}\xi_b' - \frac{\sqrt{\kappa_a}}{\rho_a}\xi_a'. \tag{A26}$$

Note that this also shows linear stability for $\delta\phi$ since $\kappa_a - \kappa_b > 0$. Now, we can go to Fourier space and solve these explicitly as in terms of the unitless susceptibility $\chi(\omega) \equiv (\frac{\kappa_a/2}{i\omega + (\kappa_a - \kappa_b)/2})$ and the pump/loss ratio $r \equiv \kappa_b/\kappa_a$:

$$\delta\phi(\omega) = \frac{\sqrt{\kappa_a}}{\rho_a} \frac{\chi(\omega)}{\kappa_a/2}(r\xi_b' - \xi_a'), \tag{A27}$$

$$\Rightarrow \phi(\omega) = \frac{\sqrt{\kappa_a}}{\rho_a} \frac{1}{i\omega}[r\chi(\omega)\xi_b' + (1 - \chi(\omega))\xi_a']. \tag{A28}$$

From here, we can finally extract the diffusion constant by considering the long time behavior of the correlation function $\langle(\phi(t) - \phi(0))^2\rangle$, where $\langle\cdot\rangle$ represents a noise average:

$$\langle(\phi(t) - \phi(0))^2\rangle = \int_{-\infty}^{\infty}(e^{i\omega t} - 1)(e^{i\omega' t} - 1)\langle\phi(\omega)\phi(\omega')\rangle \, d\omega \, d\omega'$$

$$= \frac{2\pi\kappa_a}{\rho_a^2} \int_{-\infty}^{\infty} \frac{(e^{i\omega t} - 1)(e^{i\omega' t} - 1)}{-\omega\omega'}[r^2\chi(\omega)\chi(\omega')\delta(\omega + \omega') + (1 - \chi(\omega))(1 - \chi(\omega'))\delta(\omega + \omega')] \, d\omega \, d\omega'$$

$$= \frac{4\pi\kappa_a}{\rho_a^2} \int_{-\infty}^{\infty} \frac{1 - \cos(\omega t)}{\omega^2}[r^2|\chi(\omega)|^2 + |1 - \chi(\omega)|^2] \, d\omega$$

$$= \frac{8\pi^2\kappa_a}{\rho_a^2} \frac{r^2}{(1 - r)^2}|t| \quad \text{as} \quad t \to \infty. \tag{A29}$$

This gives us the standard Schawlow-Townes phase diffusion constant, modified by the pump/loss ratio. Note that when $r \ll 1$, then

$$\frac{\kappa_a}{\rho_a^2} \frac{r^2}{(1 - r)^2} \approx \frac{\kappa_a}{\rho_a^2} r^2 = \frac{\kappa_b}{\rho_b^2}, \tag{A30}$$

which tells us that when $r \ll 1$ (and the number of photons in the b mode is much larger than the a mode), then the phase diffusion of the a mode is essentially locked to the Schawlow-Townes value of the b mode.

3. Gain saturation

The more standard interaction to stabilize a $\mathcal{PT}$ dimer that occurs often in experiments is gain saturation, where the gain rate is dependent upon the number of photons in the gain mode. This can be described using the semiclassical equations of motion

$$\partial_t a = -iJb - \frac{\kappa_a}{2}a, \tag{A31}$$

$$\partial_t b = -iJa + \frac{\kappa_b}{2}\frac{1}{1 + |b|^2/n^*}b. \tag{A32}$$

We can similarly calculate that there are two solutions: either $a = b = 0$, or

$$\frac{|a|^2}{n^*} = \frac{\kappa_a\kappa_b - 4J^2}{\kappa_a^2}, \quad \frac{|b|^2}{n^*} = \frac{\kappa_a\kappa_b - 4J^2}{4J^2}. \tag{A33}$$

At this point, we remark that in this gain saturation model, the $\mathcal{PT}$ symmetry breaking generates the instability at the linear level, but is not critical to the actual stabilization mechanism. For example, consider the limit of Eqs. (A31) and (A32) when $\kappa_a = \kappa_b \equiv \kappa$. We can now add a small detuning δ between the two modes, explicitly breaking the $\mathcal{PT}$ symmetry

of the linear dynamics. This is given by the equations of motion:

$$\partial_t a = -iJb - i\delta a - \frac{\kappa}{2}a, \tag{A34}$$

$$\partial_t b = -iJa + i\delta b + \frac{\kappa}{2}\frac{1}{1 + |b|^2/n^*}b. \tag{A35}$$

Defining the dynamical matrix to be

$$D(|b|) = \begin{pmatrix} -i\delta - \frac{\kappa}{2} & -iJ \\ -iJ & i\delta + \frac{\kappa}{2(1 + |b|^2/n^*)} \end{pmatrix}, \tag{A36}$$

then whenever $|J|, \kappa > 0$, there exists a value of $|b|$ such that the real part of the spectrum is negative definite. This can be observed by noting that when $|b| \to \infty$ there is no gain at all in the system, only loss, and so the real eigenvalues must be negative semidefinite. However, for there to be an eigenmode that is purely imaginary, then it would have to be completely localized to the a mode, which is impossible if $J \neq 0$. This tells us that the magnitude in the b mode can never grow in an unbounded way, as it will always eventually be cutoff. Thus, the system will eventually stabilize to a fixed average density, even though the $\mathcal{PT}$ symmetry is no longer present.

This is very different from the density-dependent hopping dimer in Eqs. (A13) and (A14). Adding a detuning will again explicitly break the $\mathcal{PT}$ symmetry, giving the equations of motion

$$\partial_t a = -iJ\left(1 + \frac{|a|^2 + |b|^2}{n^*}\right)b - i\delta a - \frac{\kappa}{2}a, \tag{A37}$$

$$\partial_t b = -iJ\left(1 + \frac{|a|^2 + |b|^2}{n^*}\right)a + i\delta b + \frac{\kappa}{2}b. \tag{A38}$$
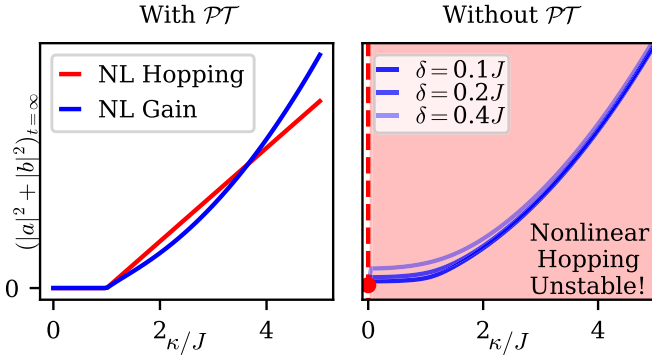
FIG. 4. On the left panel, we can see that the steady state photon number undergoes a second order transition at $\kappa = J$ for both the nonlinear hopping model [c.f., Eqs. (A37) and (A38) with $\delta = 0$] as well as the gain saturation model [c.f., Eqs. (A34) and (A35), $\delta = 0$]. On the right, when we add a detuning and break the single particle $\mathcal{PT}$ symmetry, the gain saturation model remains stable with a steady state photon density that is nearly unchanged (blue curves). On the other hand, the nonlinear hopping model is immediately unstable when $|\delta| > 0$ (red shading) unless $\kappa = 0$ (red dot). In all plots, $n^* = 5$.

Defining the linear dynamical matrix in the analogous way, we arrive at

$$D(n) = \begin{pmatrix} -i\delta - \frac{\kappa}{2} & -iJ(1 + n/n^*) \\ -iJ(1 + n/n^*) & i\delta + \frac{\kappa}{2} \end{pmatrix}, \quad \text{(A39)}$$

$$\lambda(n) = \pm\frac{1}{2}\sqrt{(2\delta - i\kappa)^2 - 4J^2(1 + n/n^*)^2}, \quad \text{(A40)}$$

with $\lambda(n)$ the complex eigenvalues. Note that one of these always has a positive real part, regardless of the density n, meaning it is always unstable. This reflects the fact that the $\mathcal{PT}$ symmetry was crucial in the stabilization mechanism, as is highlighted in the main text, and shown in Fig. 4.

4. Beyond mean field

Exact diagonalization in systems of up to order 30 steady state photons between the two modes shows that the mean field theory accurately captures the steady state photon density up to an error decaying inversely with the steady state photon number. This can be observed in Fig. 5.

APPENDIX B: CHIRAL SYMMETRY

1. SSH limit cycle solution

We can identify the limit cycle of the semiclassical equations of motion in the SSH chain as the long term solution to the dynamical equations

$$\dot{a}_i = -iJ(1 + \delta)b_i - i(1 - \delta)b_{i-1} - iU|a_i|^2 a_i + \frac{\kappa\eta^2}{2}a_i, \quad \text{(B1)}$$

$$\dot{b}_i = -iJ(1 + \delta)a_i - i(1 - \delta)a_{i+1} - iU|b_i|^2 b_i - \frac{\kappa}{2}b_i, \quad \text{(B2)}$$

where there are N different real-space a site amplitudes (a_1 through a_N) and $N - 1$ different real-space b site amplitudes (b_1 through b_{N-1}). (To make the above consistent with the
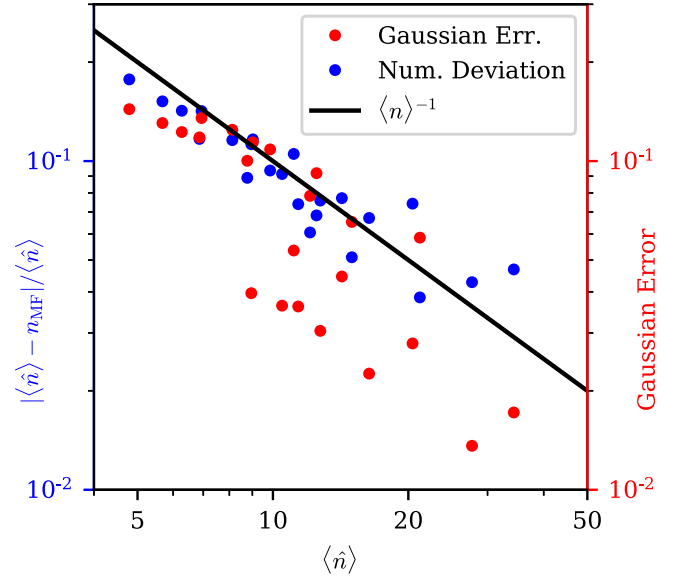

FIG. 5. Using exact numerics, we calculate (blue) the deviation in the number operator from the mean field solution. Further, we calculate (red) the error in the Gaussian approximation, which we define as $|\langle\hat{n}\hat{c}\rangle - (2\langle\hat{n}\rangle + 1)\langle\hat{c}\rangle|/\langle\hat{n}\hat{c}\rangle$, c.f., Eq. (A6). We observe both of them scale roughly as $1/\langle\hat{n}\rangle$.

boundary conditions, simply define $b_0 = b_N \equiv 0$ to get the correct equations of motion for a_1 and a_N).

We can define the vector $\vec{v} = (a_1, b_1, \ldots, b_{N-1}, a_N)^T$, and similarly the dynamical matrix $D(\vec{v})$ such that

$$\dot{\vec{v}} = D(\vec{v})\vec{v}, \quad \text{(B3)}$$

where the diagonal elements of D include the nonlinearity

$$D_{ii} = -iU|v_i|^2 + (1 - (-1)^i)\frac{\kappa\eta^2}{4} - (1 + (-1)^i)\frac{\kappa}{4}, \quad \text{(B4)}$$

and the off diagonal elements are just the SSH coupling. As in the main text, we can define the self-consistent edge mode $\vec{d}_0$, which satisfies the self-consistent eigenvalue equation

$$D(\vec{d}_0)\vec{d}_0 = i\lambda\vec{d}_0, \quad \lambda \in \mathbb{R}. \quad \text{(B5)}$$

From here, we can observe that the limit cycle solution is then simply

$$\vec{v}(t \rightarrow \infty) = e^{i\lambda t}\vec{d}_0, \quad \text{(B6)}$$

since $D(\vec{v}) = D(e^{i\phi}\vec{v}) \; \forall\phi \in \mathbb{R}$. Numerically, we find that this solution is unique and dynamically stable, as is shown in Fig. 6.

2. Gain and loss in mode basis

Recall that we can write a generic chiral symmetric Hamiltonian in the form

$$\hat{\mathcal{H}} = \sum_{i \in A, j \in B} H_{ij}\hat{a}_i^\dagger\hat{a}_j + \text{H.c.} \equiv \sum_\alpha \epsilon_\alpha \hat{d}_\alpha^\dagger \hat{d}_\alpha, \quad \text{(B7)}$$

where A, B are the sublattices. Then we can define the chiral symmetry operator $\hat{\mathcal{U}}\hat{a}_i\hat{\mathcal{U}}^\dagger = \hat{a}_i, \hat{\mathcal{U}}\hat{b}_i\hat{\mathcal{U}}^\dagger = -\hat{b}_i$. We define the unitary transformation from real space operators to
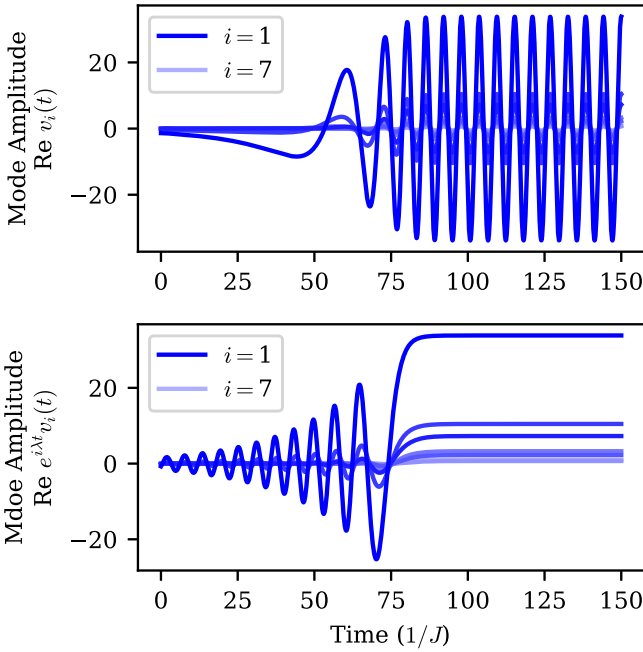
FIG. 6. This shows the time trace of the dynamical equation of motion Eq. (B3) using $J = 1$, $U = 0.001$, $\delta = 0.65$, $\kappa = 1$, $\eta = 0.2$. The left plot shows the real part of the amplitude of the dynamical vector $\vec{v}$, which begins oscillating periodiclaly time in the long time limit. The right shows the same, but in the frame rotating at the critical frequency λ defined in Eq. (B5).

Hamiltonian eigenmodes as

$$\hat{d}_\alpha \equiv \sum_i \psi_\alpha^A[i]\hat{a}_i + \psi_\alpha^B[i]\hat{b}_i. \tag{B8}$$

The chiral symmetry tells us that for every mode $\hat{d}_\alpha$, there is another mode $\hat{d}_{-\alpha}$ that is also a Hamiltonian eigenmode with opposite energy. It's expansion in real space then must be defined by

$$\hat{d}_{-\alpha} \equiv \sum_i \psi_\alpha^A[i]\hat{a}_i - \psi_\alpha^B[i]\hat{b}_i. \tag{B9}$$

We can calculate the inverse of these maps as

$$\hat{a}_i = \sum_{\alpha>0} \psi_\alpha^A[i]^*(\hat{d}_\alpha + \hat{d}_{-\alpha}), \tag{B10}$$

$$\hat{b}_i = \sum_{\alpha>0} \psi_\alpha^B[i]^*(\hat{d}_\alpha - \hat{d}_{-\alpha}), \tag{B11}$$

from unitarity. We assume that we have dissipation in the form of

$$\hat{\mathcal{L}} = \eta^2\kappa \sum_i \mathcal{D}[\hat{a}_i^\dagger] + \kappa \sum_i \mathcal{D}[\hat{b}_i]. \tag{B12}$$

Recall that the Liouvillian is unchanged under a unitary transformation of the jump operators, i.e.,

$$\sum_i \mathcal{D}[\hat{L}_i] = \sum_j \mathcal{D}\left[\sum_i U_{ji}\hat{L}_i\right], \tag{B13}$$

where U_{ij} is a unitary matrix. Therefore, we can observe the following identites:

$$\eta^2\kappa \sum_i \mathcal{D}[\hat{a}_i^\dagger] + \kappa \sum_i \mathcal{D}[\hat{b}_i] \tag{B14}$$

$$= \eta^2\kappa \sum_i \mathcal{D}\left[\sum_{\alpha>0} \psi_\alpha^A[i](\hat{d}_\alpha^\dagger + \hat{d}_{-\alpha}^\dagger)\right]$$

$$+ \kappa \sum_i \mathcal{D}\left[\sum_{\alpha>0} \psi_\alpha^B[i]^*(\hat{d}_\alpha - \hat{d}_{-\alpha})\right] \tag{B15}$$

$$= \frac{\kappa}{2} \sum_{\alpha>0} \eta^2 \mathcal{D}[\hat{d}_\alpha^\dagger + \hat{d}_{-\alpha}^\dagger] + \mathcal{D}[\hat{d}_\alpha - \hat{d}_{-\alpha}] \tag{B16}$$

$$= \frac{\kappa}{4} \sum_\alpha \eta^2 \mathcal{D}[\hat{d}_\alpha^\dagger + \hat{\mathcal{U}}\hat{d}_\alpha^\dagger\hat{\mathcal{U}}] + \mathcal{D}[\hat{d}_\alpha - \hat{\mathcal{U}}\hat{d}_\alpha\hat{\mathcal{U}}], \tag{B17}$$

recovering the result in the main text.

3. Effective nonlinear hopping

We begin by considering the weakly interacting regime, where we expect thresholdless lasing of the topological edge mode. In the main text, we gave an intuitive picture that the edge mode (localized to the A sublattice) begins to overlap strongly with the B sublattice, the instability is cut off, generating a lasing regime.

This real space picture is useful for the mean-field treatment. Alternatively, we could ask what the interaction looks like in the mode picture. As before, we define quadratic SSH Hamiltonian (but this time not distinguish between sublattices)

$$\hat{\mathcal{H}}_{\text{SSH}} = -J \sum_{i=1}^{N-1}(1 + (-1)^i\delta)\hat{a}_i^\dagger\hat{a}_{i+1} + \text{H.c.} \equiv \sum_\alpha \epsilon_\alpha \hat{d}_\alpha^\dagger\hat{d}_\alpha, \tag{B18}$$

$$\hat{d}_\alpha = \sum_i \psi_\alpha[i]\hat{a}_i, \tag{B19}$$

where we have defined the mode energy ϵ_α for the α mode, and the real space wave function profile $\psi_\alpha[i]$. Again taking the chiral symmetry to be $\hat{\mathcal{U}}$, it will be useful to define

$$\hat{d}_{-\alpha} \equiv \hat{\mathcal{U}}\hat{d}_\alpha\hat{\mathcal{U}}^\dagger \Rightarrow \epsilon_{-\alpha} = -\epsilon_\alpha, \tag{B20}$$

where we will take N to be odd so there is a singular zero mode, and let $\hat{d}_0 = \hat{\mathcal{U}}\hat{d}_0\hat{\mathcal{U}}^\dagger$. Thus, the quadratic master equation becomes

$$\partial_t\hat{\rho} = -i\sum_\alpha[\epsilon_\alpha\hat{d}_\alpha^\dagger\hat{d}_\alpha, \hat{\rho}]$$

$$+ \frac{\kappa}{4}(\mathcal{D}[\hat{d}_\alpha - \hat{d}_{-\alpha}] + \eta^2\mathcal{D}[\hat{d}_\alpha^\dagger + \hat{d}_{-\alpha}^\dagger])\hat{\rho}. \tag{B21}$$

Now, we want to expand the interaction term in this mode basis:

$$\hat{\mathcal{H}}_{\text{int}} = \frac{U}{2}\sum_i \hat{a}_i^\dagger\hat{a}_i^\dagger\hat{a}_i\hat{a}_i \sim U\sum_i \langle\hat{a}_i^\dagger\hat{a}_i\rangle\hat{a}_i^\dagger\hat{a}_i$$

$$= U\sum_{i,\alpha,\beta} \langle\hat{a}_i^\dagger\hat{a}_i\rangle\psi_\alpha[i]\psi_\beta[i]\hat{d}_\alpha^\dagger\hat{d}_\beta. \tag{B22}$$

Again, letting $\eta \ll 1$, then $\langle \hat{a}_i^\dagger \hat{a}_i \rangle \sim |\psi_0[i]|^2 \langle \hat{d}_0^\dagger \hat{d}_0 \rangle$. Next, since $\eta \ll 1$, in the steady state the bulk modes are nearly in vacuum, and so $\hat{d}_\alpha \hat{\rho}_{ss} \sim 0 \; \forall \alpha \neq 0$. Therefore, the only relevant terms in the interaction are of the form

$$\hat{\mathcal{H}}_{\text{int}} \sim U \langle \hat{d}_0^\dagger \hat{d}_0 \rangle \sum_{i,\alpha} \psi_\alpha^*[i] |\psi_0[i]|^2 \psi_0[i] \hat{d}_\alpha^\dagger \hat{d}_0, \quad \text{(B23)}$$

and so this again reduces to just density dependent hopping, this time instead of between modes in the dimer, it is between the edge modes and the lossy bulk modes of the SSH chain.

4. Topological fock states

As observed in the main text, the semiclassics breaks down when it predicts $\mathcal{O}(1)$ photons in the steady state. We will show that the steady state should instead be a topological Fock state, up to corrections that are perturbative corrections.

We will define the following quantity:

$$\xi \equiv \left(\frac{1+\delta}{1-\delta} \right), \quad \text{(B24)}$$

where the localization length $\xi_L = -[\log \xi]^{-1}$, and reparameterize $\eta = \eta' \xi^2$, where we will be taking ξ to be a small value and η' a dimensionless $\mathcal{O}(1)$ parameter.

The master equation is then

$$\partial_t \hat{\rho} = -i \sum_\alpha [\epsilon_\alpha \hat{d}_\alpha^\dagger \hat{d}_\alpha + \hat{\mathcal{H}}_{\text{int}}, \hat{\rho}]$$

$$+ \frac{\kappa}{4} (\mathcal{D}[\hat{d}_\alpha - \hat{d}_{-\alpha}] + \eta'^2 \xi^4 \mathcal{D}[\hat{d}_\alpha^\dagger + \hat{d}_{-\alpha}^\dagger]) \hat{\rho}. \quad \text{(B25)}$$

Now, we first consider the scenario when $\eta' = 0$. In this case, we have only loss, and there are exactly two degenerate steady states. These are the vacuum $\hat{\rho}_0 \equiv |0\rangle\langle 0|$ and $\hat{\rho}_1 \equiv \hat{d}_0^\dagger |0\rangle\langle 0| \hat{d}_0$ the singly excited edge mode Fock state, which is a steady state because it sees no loss. We cannot, however, add more excitations because the interaction tells us these are no longer eigenmodes of the Hamiltonian.

Now, we turn on η'. To zeroth order, we assume that the perturbation does nothing except within the degenerate steady space manifold. Limiting ourselves to just these two pure states, all the gain wants to do it pump photons from the vacuum into the single Fock state $\hat{\rho}_1$, which becomes now the nondegenerate steady state.

To next order, we need to consider the possibility that the pumping can push $\hat{\rho}_1$ into the doubly excited subspace. However, because $\hat{\rho}_2 \equiv \hat{d}_0^\dagger \hat{\rho}_1 \hat{d}_0$ does not commute with the Hamiltonian, it has a finite lifetime. Now, we will calculate the different decay rates and channels to leave the doubly excited manifold. Before doing so, it is critical to observe that, by making the localization length small, we make it difficult for the edge mode to tunnel into any other mode:

$$\psi_0[i] = \sqrt{1-\xi^2} \sin(\pi i/2) \xi^{(i-1)/2}, \quad \text{(B26)}$$

$$\sum_{\alpha \neq 0} |\langle 0| \hat{d}_\alpha \hat{d}_0 \hat{\mathcal{H}} \hat{d}_0^\dagger \hat{d}_0^\dagger |0\rangle|$$

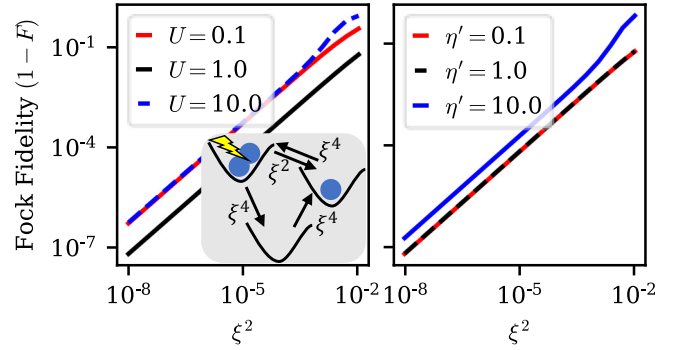$$= \frac{U}{2} \sum_{\alpha \neq 0, i} |\psi_\alpha[i] \psi_0[i]^3|$$

FIG. 7. Scaling of the Fock fidelity versus the unitless hopping asymmetry ξ, which is also related to the localization length, for various values of U (left) or η' (right). Note the predicted quadratic scaling, as well as the strong robustness to parameters. Here, $\eta \equiv \eta' \xi^2$, $U = J = \kappa = 1$ unless otherwise specified in the plot. Inset: Schematic depicting the Fock stabilization mechanism and scaling properties.

$$= \frac{U}{2} |\psi_0[0]|^3 |\sum_{\alpha \neq 0} |\psi_\alpha[0]| + \mathcal{O}(\xi^3)$$

$$= \mathcal{O}(\xi). \quad \text{(B27)}$$

Where the key observation is that the overlap of the edge mode on the first lattice site is $|\psi_0[1]|^2 = 1 - \xi^2$, and so by the unitarity of the transformation, $\sum_{\alpha \neq 0} |\psi_\alpha[1]|^2 = \xi^2$, and so $\sum_{\alpha \neq 0} |\psi_\alpha[0]| = \mathcal{O}(\xi)$. Now, we can begin to do power counting in powers of ξ. For the Liouvillian to map $\hat{\rho}_2 \to \hat{\rho}_1$, the nonlinearity must act on both sides of the density matrix to move density from the zero mode to any other eigenmode making it an $\mathcal{O}(\xi^2)$ process. The linear loss dissipation can then move this population back to vacuum. Alternatively, the nonlinearity must act twice on both sides of the density matrix to transfer population from the doubly excited state so having no density on the edge mode, which can then decay back to vacuum, which is therefore an $\mathcal{O}(\xi^4)$ process. Denoting ρ_i to be the probability to be in state $\hat{\rho}_i$, we can define the rate equations (just keeping power of ξ)

$$\dot{\rho}_0 = -\xi^4 \rho_0 + \xi^4 \rho_2, \quad \text{(B28)}$$

$$\dot{\rho}_1 = \xi^4 \rho_0 + \xi^2 \rho_2 - \xi^4 \rho_1, \quad \text{(B29)}$$

$$\dot{\rho}_2 = \xi^4 \rho_1 - (\xi^4 + \xi^2) \rho_2. \quad \text{(B30)}$$

These three equations sum to zero (as expected by the conservation of probability). Solving them gives

$$\rho_1 = \frac{\xi^2 + \xi^4}{\xi^2 + 3\xi^4} = 1 - 2\xi^2 + O(\xi^4), \quad \text{(B31)}$$

$$\rho_0 = \rho_2 = \frac{\xi^4}{\xi^2 + 3\xi^4} = \xi^2 + O(\xi^4). \quad \text{(B32)}$$

This somewhat heuristic argument is sufficient to perfectly capture the scaling with ξ (c.f., Fig. 7).

We now wish to show that this cannot be reduced to any simple effective, Markovian, single-mode dynamics. Therefore, one cannot use any combination of single-photon pumping, single- or two-photon loss, or any number-conserving
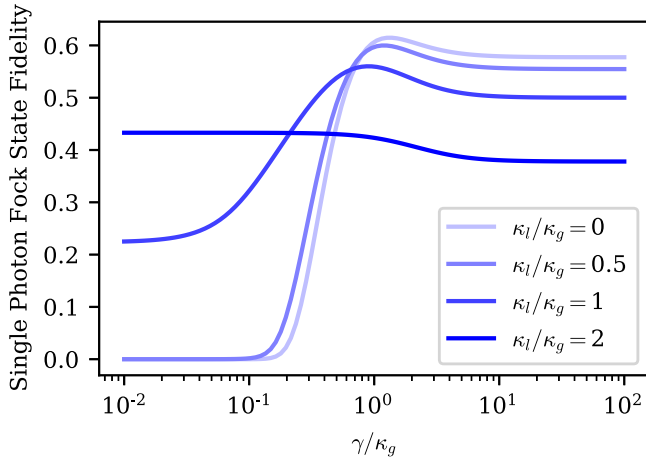
FIG. 8. This shows the fidelity of the steady state of the master equation in Eq. (B34) as a function of γ/κ_g for varying values of κ_l/κ_g. Note the optimal value of $\kappa_l = 0$, and $\gamma \sim \kappa_g$, which gives a fidelity of around 0.6.

Hamiltonian nonlinearity to stabilize a single photon Fock state. Consider the single-mode quantum master equation

$$\dot{\rho} = \hat{\mathcal{L}}\hat{\rho}, \quad (B33)$$

$$\hat{\mathcal{L}} = -i\left[\Delta\hat{n} + \frac{U}{2}\hat{n}^2, \bullet\right] + \kappa_g \mathcal{D}[\hat{a}^\dagger] + \kappa_l \mathcal{D}[\hat{a}] + \gamma \mathcal{D}[\hat{a}^2], \quad (B34)$$

with $\hat{n} \equiv \hat{a}^\dagger\hat{a}$. Firstly, we can observe that we have a $U(1)$ weak symmetry generated by total photon number $\hat{n}$ [59]. Hence, the steady state ρ_{ss} defined by $\hat{\mathcal{L}}\rho_{ss} = 0$ commutes with $\hat{n}$. Because the Hamiltonian $\hat{\mathcal{H}} = \Delta\hat{n} + \frac{U}{2}\hat{n}^2$ is only a function of $\hat{n}$, this means the steady state is completely independent of the parameters Δ, U, and so without loss of generality we can set them to be zero. Thus, we only need consider the dissipative part of the dynamics. There are two dimensionless parameters γ/κ_g and κ_l/κ_g, and we can observe that, after optimizing over these, the fidelity to a single photon Fock state never reaches above $\sim$0.6, see Fig. 8.
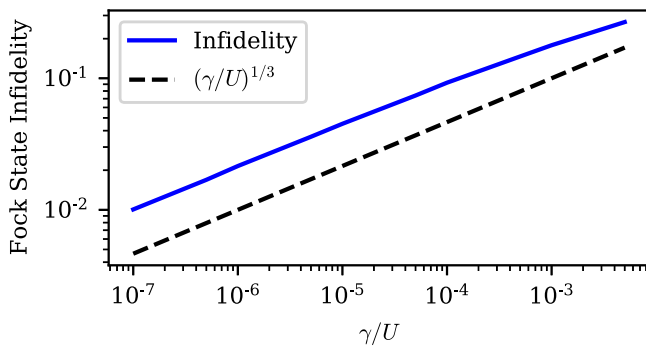

FIG. 9. Fock state infidelity $1 - F$ as a function of additional loss on the B sublattice [c.f., Eq. (B35)]. This shows a fixed value of the nonlinearity $U = J = 1$, and optimizing over the A-sublattice loss rate κ, the gain/loss ratio η, and the hopping asymmetry ξ. The dotted line is a guide to the eye, showing power law decay $(\gamma/U)^{1/3}$.
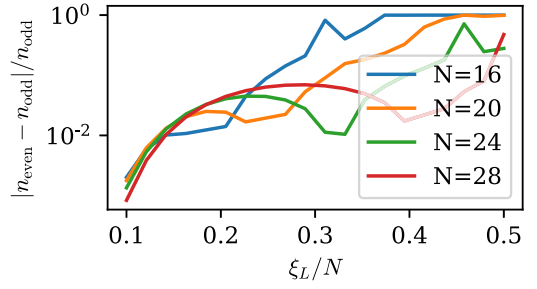

FIG. 10. We look at mean-field dynamics of pairs of SSH chains of length N and $N + 1$. We define n_{even} (n_{even}) to be the steady state photon total photon number of the chain of length N ($N + 1$), for $N = 16, 20, 24, 28$. We find that as the localization length ξ_L/N becomes small compared to system size, the results converge to give the same result, as expected. Parameters used here are $\kappa = J = 1$ and $\eta = U = 0.1$, but the results are general across parameter regimes.

5. Robustness to additional loss

In this section, we will consider the robustness of the topological edge mode Fock state stabilization to unwanted loss on the B sublattice. We will model this as

$$\dot{\rho} = -i[\hat{\mathcal{H}}_{\text{SSH}} + \hat{\mathcal{H}}_{\text{int}}, \hat{\rho}] + \kappa \sum_{i \in A} \mathcal{D}[\hat{a}_i]\hat{\rho}$$

$$+ \kappa\eta^2 \sum_{i \in B} \mathcal{D}[\hat{a}_i^\dagger]\hat{\rho} + \gamma \sum_{i \in B} \mathcal{D}[\hat{a}_i]\hat{\rho}, \quad (B35)$$

where $\hat{\mathcal{H}}_{\text{SSH}}$ is defined in Eq. (B19) and $\hat{\mathcal{H}}_{\text{int}} = \frac{U}{2}\sum_i \hat{a}_i^\dagger\hat{a}_i^\dagger\hat{a}_i\hat{a}_i$ is the same on-site Kerr nonlinearities we have been considering throughout. If we hold the nonlinearity $U = J = 1$ fixed and optimize over the remaining parameters (κ, η, ξ), we can see that the Fock state infidelity grows monotonically with the B lattice loss rate γ with a power law that appears to scale roughly as $(\gamma/U)^{1/3}$ see Fig. 9.

6. Even-length SSH chains

Throughout the manuscript and Supplemental Material, we have considered SSH chains of an odd number of sites because they have an exact zero mode localized to a single sublattice, simplifying both calculations and our intuition. For
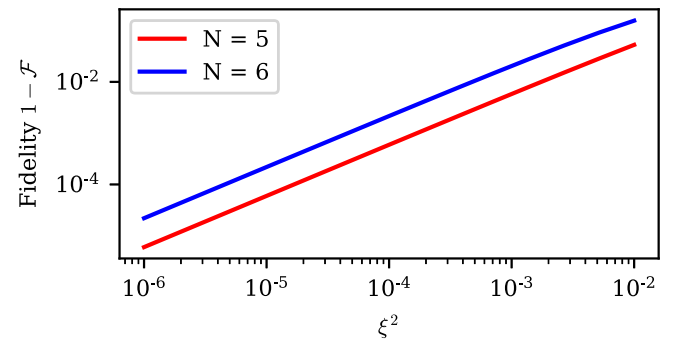

FIG. 11. This is a recreation of the data shown in Fig. 6, except now we look at the case of an even length ($N = 6$) and odd length ($N = 5$) chain. We take values $\eta = \xi^2$, $U = J = \kappa = 1$ as before, and observe the same scaling. Note that the even length chain has slightly lower fidelity than odd.

an SSH chain with an even number of lattice sites, there exist two edge modes that live on opposite sides of the chain. They hybridize extremely weakly under the Hamiltonian, so that the symmetric and antisymmetric combinations are the true Hamiltonian eigenmodes, which technically live on both sublattices. The strength of this hybridization decays exponentially with the edge mode localization length, as the Hamiltonian is local, and so the edge modes become degenerate zero modes in the thermodynamic limit. More concretely, if the localization length ξ_L is much smaller than the system size,

$$\frac{\xi_L}{N} = -\left[N \log \left(\frac{1-\delta}{1+\delta} \right) \right]^{-1} \ll 1, \qquad \text{(B36)}$$

then we claim that the even and odd chain lengths should be indistinguishable. This is because the relaxation dynamics occur exponentially faster than the system can realize that the edge is no longer a true eigenmode. We confirm this with mean-field dynamics in Fig. 10.

Similarly, we can ask how the even and odd length chains differ in the Fock state regime. We can run exact diagonalization on small systems to see how the fidelity to a Fock state varies as we tune $\xi = (1 - \delta)/(1 + \delta)$. Here, we see that both even and odd chains have the same scaling parameter where the (in)fidelity scales proportionally to ξ^2. However, the odd numbered chain has a larger prefactor, indicating that it does slightly poorer than the odd numbered case (as expected), but that it scales asymptotically in the same manner. This is shown in Fig. 11.

[1] D. Walls and G. Milburn, *Quantum Optics* (Springer-Verlag, New York, 1994).

[2] C. Gardiner and P. Zoller, *Quantum Noise: A Handbook of Markovian and non-Markovian Quantum Stochastic Methods with Applications to Quantum Optics*, Springer Series in Synergetics (Springer, Berlin, 2004).

[3] J. A. Acebrón, L. L. Bonilla, C. J. Pérez Vicente, F. Ritort, and R. Spigler, The Kuramoto model: A simple paradigm for synchronization phenomena, Rev. Mod. Phys. **77**, 137 (2005).

[4] S. N. Dorogovtsev, A. V. Goltsev, and J. F. F. Mendes, Critical phenomena in complex networks, Rev. Mod. Phys. **80**, 1275 (2008).

[5] L. M. Sieberer, S. D. Huber, E. Altman, and S. Diehl, Dynamical critical phenomena in driven-dissipative systems, Phys. Rev. Lett. **110**, 195301 (2013).

[6] S. Diehl, A. Micheli, A. Kantian, B. Kraus, H. P. Büchler, and P. Zoller, Quantum states and phases in driven open quantum systems with cold atoms, Nat. Phys. **4**, 878 (2008).

[7] S. Diehl, A. Tomadin, A. Micheli, R. Fazio, and P. Zoller, Dynamical phase transitions and instabilities in open atomic many-body systems, Phys. Rev. Lett. **105**, 015702 (2010).

[8] I. Carusotto and C. Ciuti, Quantum fluids of light, Rev. Mod. Phys. **85**, 299 (2013).

[9] M. H. Szymańska, J. Keeling, and P. B. Littlewood, Nonequilibrium quantum condensation in an incoherently pumped dissipative system, Phys. Rev. Lett. **96**, 230602 (2006).

[10] J. Lebreuilly, A. Biella, F. Storme, D. Rossini, R. Fazio, C. Ciuti, and I. Carusotto, Stabilizing strongly correlated photon fluids with non-Markovian reservoirs, Phys. Rev. A **96**, 033828 (2017).

[11] O. Scarlatella, R. Fazio, and M. Schiró, Emergent finite frequency criticality of driven-dissipative correlated lattice bosons, Phys. Rev. B **99**, 064511 (2019).

[12] R. Ma, B. Saxberg, C. Owens, N. Leung, Y. Lu, J. Simon, and D. I. Schuster, A dissipatively stabilized Mott insulator of photons, Nature (London) **566**, 51 (2019).

[13] M. Hafezi, P. Adhikari, and J. M. Taylor, Chemical potential for light by parametric coupling, Phys. Rev. B **92**, 174305 (2015).

[14] R. Ma, C. Owens, A. Houck, D. I. Schuster, and J. Simon, Autonomous stabilizer for incompressible photon fluids and solids, Phys. Rev. A **95**, 043811 (2017).

[15] B. van der Pol, LXXXVIII. on 'Relaxation-Oscillations", London, Edinburg, Dublin Philos. Mag. J. Sci. **2**, 978 (1926).

[16] C. M. Bender and S. Boettcher, Real spectra in non-Hermitian Hamiltonians having $\mathcal{PT}$ symmetry, Phys. Rev. Lett. **80**, 5243 (1998).

[17] C. M. Bender, Making sense of non-Hermitian Hamiltonians, Rep. Prog. Phys. **70**, 947 (2007).

[18] L. Feng, Z. J. Wong, R.-M. Ma, Y. Wang, and X. Zhang, Single-mode laser by parity-time symmetry breaking, Science **346**, 972 (2014).

[19] B. Peng, S. K. Özdemir, F. Lei, F. Monifi, M. Gianfreda, G. L. Long, S. Fan, F. Nori, C. M. Bender, and L. Yang, Parity–time-symmetric whispering-gallery microcavities, Nat. Phys. **10**, 394 (2014).

[20] L. Ge and R. El-Ganainy, Nonlinear modal interactions in parity-time (pt) symmetric lasers, Sci. Rep. **6**, 24889 (2016).

[21] H. Hodaei, M.-A. Miri, M. Heinrich, D. N. Christodoulides, and M. Khajavikhan, Parity-time–symmetric microring lasers, Science **346**, 975 (2014).

[22] R. El-Ganainy, K. G. Makris, M. Khajavikhan, Z. H. Musslimani, S. Rotter, and D. N. Christodoulides, Non-Hermitian physics and PT symmetry, Nat. Phys. **14**, 11 (2018).

[23] A. P. Schnyder, S. Ryu, A. Furusaki, and A. W. W. Ludwig, Classification of topological insulators and superconductors in three spatial dimensions, Phys. Rev. B **78**, 195125 (2008).

[24] B. Hu, Z. Zhang, H. Zhang, L. Zheng, W. Xiong, Z. Yue, X. Wang, J. Xu, Y. Cheng, X. Liu, and J. Christensen, Non-Hermitian topological whispering gallery, Nature (London) **597**, 655 (2021).

[25] M. Seclì, T. Ozawa, M. Capone, and I. Carusotto, Spatial and spectral mode-selection effects in topological lasers with frequency-dependent gain, APL Photonics **6**, 050803 (2021).

[26] P. St-Jean, V. Goblot, E. Galopin, A. Lemaître, T. Ozawa, L. Le Gratiet, I. Sagnes, J. Bloch, and A. Amo, Lasing in topological edge states of a one-dimensional lattice, Nat. Photonics **11**, 651 (2017).

[27] M. Parto, S. Wittek, H. Hodaei, G. Harari, M. A. Bandres, J. Ren, M. C. Rechtsman, M. Segev, D. N. Christodoulides, and M. Khajavikhan, Edge-mode lasing in 1D topological active arrays, Phys. Rev. Lett. **120**, 113901 (2018).

[28] H. Zhao, P. Miao, M. H. Teimourpour, S. Malzard, R. El-Ganainy, H. Schomerus, and L. Feng, Topological hybrid silicon microlasers, Nat. Commun. **9**, 981 (2018).

[29] S. Mittal, E. A. Goldschmidt, and M. Hafezi, A topological source of quantum light, Nature (London) **561**, 502 (2018).

[30] A. Blanco-Redondo, B. Bell, D. Oren, B. J. Eggleton, and M. Segev, Topological protection of biphoton states, Science **362**, 568 (2018).

[31] J. C. Owens, M. G. Panetta, B. Saxberg, G. Roberts, S. Chakram, R. Ma, A. Vrajitoarea, J. Simon, and D. I. Schuster, Chiral cavity quantum electrodynamics, Nat. Phys. **18**, 1048 (2022).

[32] G. Lindblad, On the generators of quantum dynamical semigroups, Commun. Math. Phys. **48**, 119 (1976).

[33] V. Gorini, A. Kossakowski, and E. C. G. Sudarshan, Completely positive dynamical semigroups of n-level systems, J. Math. Phys. **17**, 821 (1976).

[34] K. V. Kepesidis, T. J. Milburn, J. Huber, K. G. Makris, S. Rotter, and P. Rabl, PT-symmetry breaking in the steady state of microscopic gain–loss systems, New J. Phys. **18**, 095003 (2016).

[35] F. Roccati, S. Lorenzo, G. Massimo Palma, G. T. Landi, M. Brunelli, and F. Ciccarello, Quantum correlations in PT-symmetric systems, Quantum Sci. Technol. **6**, 025005 (2021).

[36] J. Hirsch, Bond-charge repulsion and hole superconductivity, Physica C **158**, 326 (1989).

[37] M. Maik, P. Hauke, O. Dutta, M. Lewenstein, and J. Zakrzewski, Density-dependent tunneling in the extended Bose–Hubbard model, New J. Phys. **15**, 113041 (2013).

[38] Y. Hadad, A. B. Khanikaev, and A. Alù, Self-induced topological transitions and edge states supported by nonlinear staggered potentials, Phys. Rev. B **93**, 155112 (2016).

[39] J. Wiersig, Enhancing the sensitivity of frequency and energy splitting detection by using exceptional points: Application to microcavity sensors for single-particle detection, Phys. Rev. Lett. **112**, 203901 (2014).

[40] W. Chen, S. Kaya Özdemir, G. Zhao, J. Wiersig, and L. Yang, Exceptional points enhance sensing in an optical microcavity, Nature (London) **548**, 192 (2017).

[41] H. Hodaei, A. U. Hassan, S. Wittek, H. Garcia-Gracia, R. El-Ganainy, D. N. Christodoulides, and M. Khajavikhan, Enhanced sensitivity at higher-order exceptional points, Nature (London) **548**, 187 (2017).

[42] H.-K. Lau and A. A. Clerk, Fundamental limits and non-reciprocal approaches in non-Hermitian quantum sensing, Nat. Commun. **9**, 4320 (2018).

[43] M. Zhang, W. Sweeney, C. W. Hsu, L. Yang, A. D. Stone, and L. Jiang, Quantum noise theory of exceptional point amplifying sensors, Phys. Rev. Lett. **123**, 180501 (2019).

[44] C. Chen, L. Jin, and R.-B. Liu, Sensitivity of parameter estimation near the exceptional point of a non-Hermitian system, New J. Phys. **21**, 083002 (2019).

[45] A. McDonald and A. A. Clerk, Exponentially enhanced quantum sensing with non-Hermitian lattice dynamics, Nat. Commun. **11**, 5382 (2020).

[46] S. Zippilli, J. Li, and D. Vitali, Steady-state nested entanglement structures in harmonic chains with single-site squeezing manipulation, Phys. Rev. A **92**, 032319 (2015).

[47] S. Ma, M. J. Woolley, I. R. Petersen, and N. Yamamoto, Pure gaussian states from quantum harmonic oscillator chains with a single local dissipative process, J. Phys. A: Math. Theor. **50**, 135301 (2017).

[48] Y. Yanay and A. A. Clerk, Reservoir engineering of bosonic lattices using chiral symmetry and localized dissipation, Phys. Rev. A **98**, 043615 (2018).

[49] S. Zippilli and D. Vitali, Dissipative engineering of gaussian entangled states in harmonic lattices with a single-site squeezed reservoir, Phys. Rev. Lett. **126**, 020402 (2021).

[50] A. Pocklington, Y.-X. Wang, and A. A. Clerk, Dissipative pairing interactions: Quantum instabilities, topological light, and volume-law entanglement, Phys. Rev. Lett. **130**, 123602 (2023).

[51] V. Peano, M. Houde, C. Brendel, F. Marquardt, and A. A. Clerk, Topological phase transitions and chiral inelastic transport induced by the squeezing of light, Nat. Commun. **7**, 10779 (2016).

[52] W. P. Su, J. R. Schrieffer, and A. J. Heeger, Solitons in polyacetylene, Phys. Rev. Lett. **42**, 1698 (1979).

[53] W. P. Su, J. R. Schrieffer, and A. J. Heeger, Soliton excitations in polyacetylene, Phys. Rev. B **22**, 2099 (1980).

[54] E. Kim, X. Zhang, V. S. Ferreira, J. Banker, J. K. Iverson, A. Sipahigil, M. Bello, A. González-Tudela, M. Mirhosseini, and O. Painter, Quantum electrodynamics in a topological waveguide, Phys. Rev. X **11**, 011015 (2021).

[55] Y. Gong, L. Guo, S. Wong, A. J. Bennett, and S. S. Oh, Tailoring topological edge states with photonic crystal nanobeam cavities, Sci. Rep. **11**, 1055 (2021).

[56] D. Leykam and L. Yuan, Topological phases in ring resonators: Recent progress and future prospects, Nanophotonics **9**, 4473 (2020).

[57] A. Youssefi, S. Kono, A. Bancora, M. Chegnizadeh, J. Pan, T. Vovk, and T. J. Kippenberg, Topological lattices realized in superconducting circuit optomechanics, Nature (London) **612**, 666 (2022).

[58] F. Yang, P. Molignini, and E. J. Bergholtz, Dissipative boundary state preparation, Phys. Rev. Res. **5**, 043229 (2023).

[59] B. Buča and T. Prosen, A note on symmetry reductions of the lindblad equation: transport in constrained open spin chains, New J. Phys. **14**, 073007 (2012).